

# Self-Sealed Bionic Long Microchannels with Thin Walls and Designable Nanoholes Prepared by Line-Contact Capillary-Force Assembly

Zhao-Xin Lao, Yan-Lei Hu,\* Deng Pan, Ren-Yan Wang, Chen-Chu Zhang, Jin-Cheng Ni, Bing Xu, Jia-Wen Li, Dong Wu,\* and Jia-Ru Chu

*Long microchannels with thin walls, small width, and nanoholes or irregular shaped microgaps, which are similar to capillaries or cancerous vessels, are urgently needed to simulate the physiological activities in human body. However, the fabrication of such channels remains challenging. Here, microchannels with designable holes are manufactured by combining laser printing with line-contact capillary-force assembly. Two microwalls are first printed by femtosecond laser direct-writing, and subsequently driven to collapse into a channel by the capillary force that arises in the evaporation of developer. The channel can remain stable in solvent due to the enhanced Van der Waals' force caused by the line-contact of microwalls. Microchannels with controllable nanoholes and almost arbitrary patterns can be fabricated without any bonding or multistep processes. As-prepared microchannels, with wall thicknesses less than 1  $\mu\text{m}$ , widths less than 3  $\mu\text{m}$ , lengths more than 1 mm, are comparable with human capillaries. In addition, the prepared channels also exhibit the ability to steer the flow of liquid without any external pump.*

Capillaries transport nutrients and metabolites for human physiological activities and distribute everywhere in human body. Bionic capillaries, which allow people to simulate the biochemical reactions in human body, is of considerable interest for emerging applications in microfluidics,<sup>[1]</sup> biomedical devices self-healing,<sup>[2]</sup> and tissue engineering.<sup>[3]</sup> There are mainly three types of blood capillaries (i.e., continuous, fenestrated and sinusoidal). Therein, fenestrated capillaries were covered with nanoholes to exchange substance

with organs. Besides, sinusoidal capillaries and cancerous vessels always contain a large number of irregular intercellular gaps and holes with arbitrary shapes and sizes. Therefore, it is obviously important to manufacture such microchannels with designable nanoholes and controllable sizes similar to human capillaries.

Recent years have witnessed a rapid increasing demand of microchannels in micro/nanofluidic devices because of their important applications in many fields, such as microfluidic devices,<sup>[4]</sup> chemical analyses,<sup>[5]</sup> micropumps,<sup>[6]</sup> and microsensors.<sup>[7]</sup> Correspondingly, many fabrication strategies have been proposed to create high-quality microchannels, for example, photolithography,<sup>[6,7]</sup> direct laser writing,<sup>[8,9]</sup> self-rolled-up driven by stressed nanomembrane,<sup>[10]</sup> photo-induced polymerization caused by direct laser writing,<sup>[11]</sup> diffraction,<sup>[12]</sup> or special light field.<sup>[13]</sup> Despite these strategies can create channels range from tens to hundreds of micrometers in width, smaller-width (<10  $\mu\text{m}$ ) microchannels with controllable shape are required in many important biological researches, such as exploring the behaviors of cells in restricted microenvironment.<sup>[1,9,10]</sup> However, there is still

Z.-X. Lao, Dr. Y.-L. Hu, D. Pan, R.-Y. Wang,  
Dr. C.-C. Zhang, J.-C. Ni, B. Xu,  
Dr. J.-W. Li, Prof. D. Wu, Prof. J.-R. Chu  
CAS Key Laboratory of Mechanical Behavior  
and Design of Materials  
Department of Precision Machinery and  
Precision Instrumentation  
University of Science and Technology of China  
Hefei 230026, China  
E-mail: huyl@ustc.edu.cn; dongwu@ustc.edu.cn



DOI: 10.1002/sml.201603957

a lack of a simple method to realize nanoholes-decorated microchannels with dimensions equivalent to human capillaries, whose widths are less than 10  $\mu\text{m}$ , lengths vary from several micrometers to several millimeters, and thicknesses are only about 1  $\mu\text{m}$ .

Capillary force driven self-assembly has attracted great attention because of its low cost, simplicity, and scalability.<sup>[14–16]</sup> A variety of microstructures have been created by the combination of capillary force self-assembly and top-down techniques, for example, conventional photolithography,<sup>[14]</sup> replica molding,<sup>[14]</sup> multibeam laser interference lithography,<sup>[16]</sup> and electron beam lithography (EBL).<sup>[17]</sup> However, these microstructures are reversible because of the weak Van der Waals' force based on "point-contact" of pillars. Here, we demonstrated a kind of special microchannels consisting of two polymer walls structured by femtosecond laser direct-writing and line-contact capillary-force assembly (LC-CFA) method. Without any bonding or multistep processes, microchannels with designed nanoholes and gaps, whose wall thickness less than 1  $\mu\text{m}$ , width less than 3  $\mu\text{m}$  and length more than 1 millimeter are created and exhibit the ability to steer flow of liquid without any external pump. The combination of femtosecond laser (fs-laser) printing technique with LC-CFA in our approach leads to a simple, rapid, flexible, facile strategy to prepare microchannels.

The fabrication process of microchannels based on the enhanced "line-contact" Van der Waals' force is described schematically in **Scheme 1**. In this experiment, NOA61 (Norland, USA) is chosen as the photo-polymerization material due to its excellent elasticity compared with the SZ2080 photoresist (IESL-FORTH, Greece) used in our previous works.<sup>[18]</sup> Microwalls, whose location and height can be accurately determined by the nanotranslation stage (PI, E545), are readily fabricated by focusing a femtosecond laser (Ti:sapphire, Chameleon vision-S, Coherent, wavelength 800 nm, repetition rate 80 MHz and pulse duration 75 fs) beam into the photosensitive polymer with an objective lens (50 $\times$ , numerical aperture (NA) = 0.8). Subsequently, the sample is developed in acetone as shown in Scheme 1. Then, evaporation appears after taking the sample out from developer. A meniscus arises between two microwalls when the liquid surface reaches the top of microwalls which leads to asymmetric capillary force and results in microchannels finally.

As is shown in **Figure 1a**, a meniscus arises between two micropillars/walls when the liquid evaporates, which leads to a capillary force. The self-assembled microstructures are a result of the competition between capillary force ( $F_c$ ) and standing force ( $F_s$ ). After assembly, what resist  $F_s$  to hold

the structures is the Van der Waals' force ( $F_v$ ) that appears when the tops of micropillars/walls are in contact. When we immerse the assembled structures in liquid again,  $F_v$  decreases, resulting in two probable results: the structures unfold again ( $F_s > F_v$ ) or still keep closed ( $F_s < F_v$ ). Figure 1b shows the difference in principle between capillary-driven self-assembled micropillars and microchannels. The contact area of microchannel changed from tip-contact into line-contact, leading to a larger  $F_v$  that ensures the assembled channels keep stable in liquid. Figure 1c,d shows scanning electron microscope (SEM) images of microchannels created in this way, which indicate that the surface of self-assembled microchannel is homogeneous.

The inset of **Figure 2a** depicts the main factors of a microwall, including length ( $L$ ), height ( $H$ ), thickness ( $t$ ) and the space between two approaching microwalls ( $W$ ). In order to ignore the influence between two cells, the distance between two individual cells is designed twice larger than the internal spacing in a cell. Meanwhile, the cross-section of the microwall is simplified as a rectangle with lengths of  $t$  and  $L$ . As the developer evaporates to the level of the freestanding tips, a meniscus is formed between neighboring walls, yielding a capillary force along the tangent of meniscus:

$$F_c \sim \frac{HL\gamma\cos\theta}{W} \quad (1)$$

which is proportional to the interfacial tension  $\gamma$  of the solvent, the height  $H$ , the length  $L$  of walls, the cosine of contact angle  $\theta$ , and inversely proportional to the spacing width  $W$  between adjacent walls, as shown in inset of Figure 1a. Resistance to the capillary force is the bending ability of pillars, giving rise to an elastic restoring force upon contact at their tips:

$$F_s \sim E \frac{t^3 LW}{H^3} \quad (2)$$

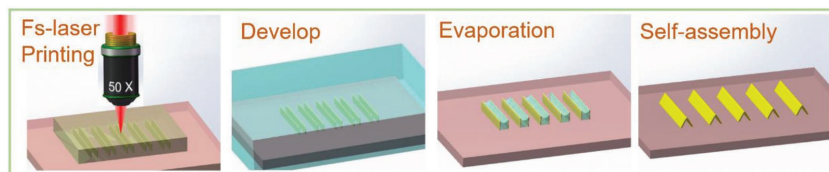
where  $E$  is the Young's modulus.

There is no doubt that  $F_v$  is proportional to the contact area of two walls. Assuming that the height of contact region is  $h_a$ , there is:

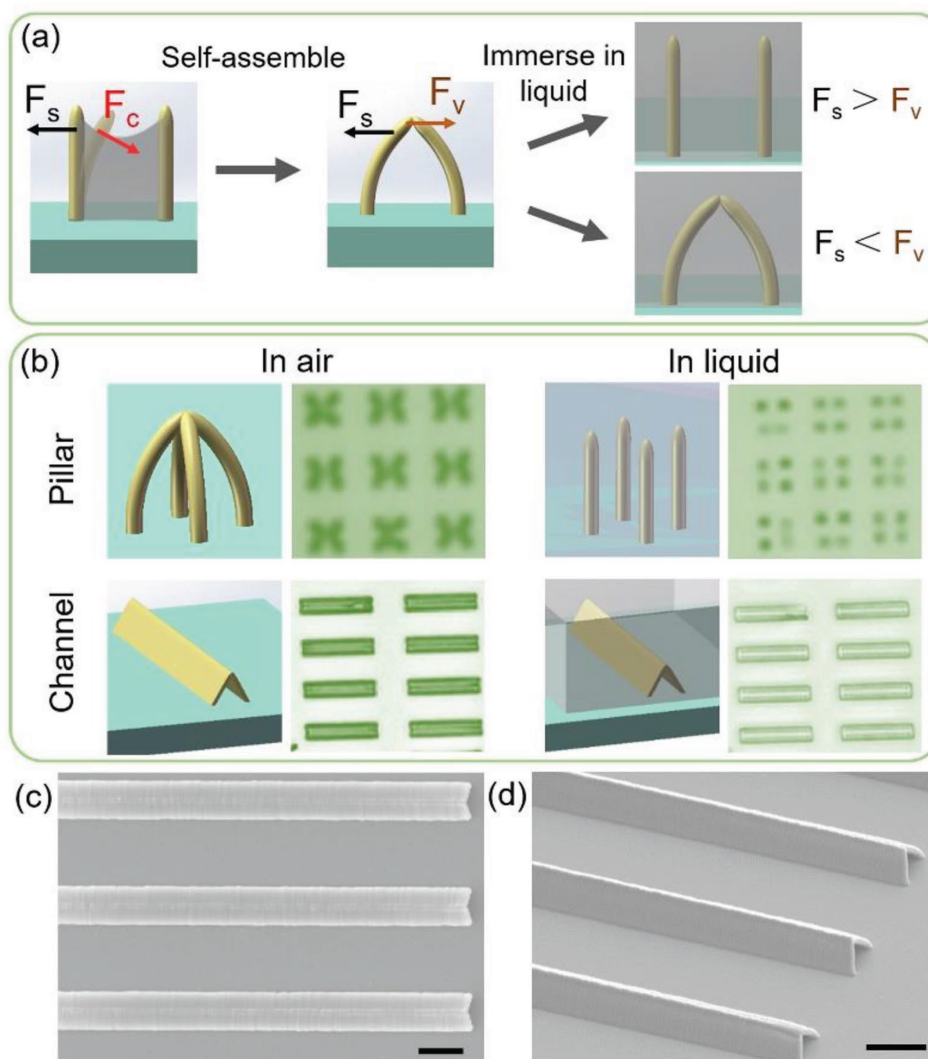
$$F_v \sim S_a = L \cdot h_a \quad (3)$$

Compared with our previous work,<sup>[18,19]</sup> the capillary-driven self-assembly channel here keeps stable because of the increased  $L$  and  $h_a$ . In our experiment, the channel does not open in liquid. (More discussion is shown in the Supporting Information.)

Figure 2a indicates that the thickness of microchannel ranges from 400 to 800 nm due to different laser energy and exposure time, which is similar to the thickness of human capillaries. It is worth mentioning that the thickness can be further decreased by using objective lens with a higher NA or increased by repetitive scanning processing of laser printing. Figure 2b exhibits the dependency map of assembly on different length



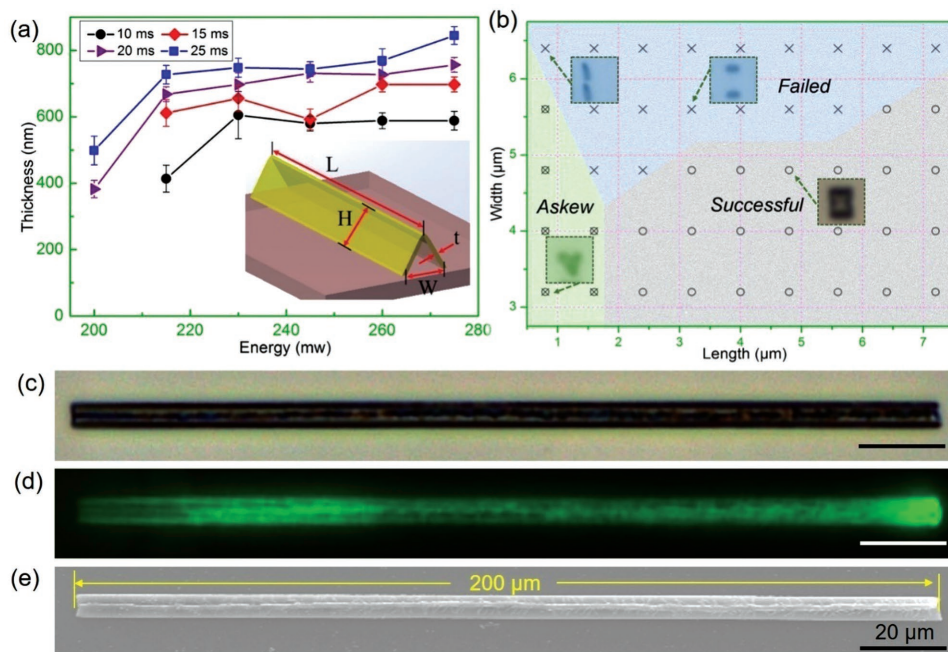
**Scheme 1.** The fabrication process of LPCS microchannels. Microwalls were printed by femtosecond laser first and developed in acetone. A meniscus arises between two microwalls when the liquid surface reaches the top of microwalls, which leads to asymmetric capillary force and results in microchannels finally.



**Figure 1.** Self-sealed microchannels fabricated by enhanced capillary force and Van der Waals' force based on line-contact. a) Capillary-driven self-assembly is a result of the competition between the standing force ( $F_s$ ) and capillary force ( $F_c$ ). And, after assembling, the hold of microstructures relies on Van der Waals' force ( $F_v$ ). When immersed assembled structures in liquid,  $F_v$  decreases which will lead to two different results: the structures unfold again ( $F_s > F_v$ ) or still hold ( $F_s < F_v$ ). b) The sketches and corresponding microscope images of different capillary-driven assembled structures in air and liquid. Microstructures assembled by pillars will unfold again when being immersed in liquid. However, for microchannels assembled by microwalls, increased contact area causes bigger  $F_v$  which ensures that assembled microchannel still fold when immersed in liquid again. c, d) The SEM images (top view and tilted view, 45°) of self-assembled microchannels. Scale bars: 5 μm.

(0.7–7 μm) and width (3.2–6.4 μm) when height and thickness are fixed (here,  $H = \approx 4.5$  μm,  $t = \approx 700$  nm). This map can be divided into three areas, in which the insets are typical optical images of different experimental results. When the length is small (green area), microwall changes into micropillar which is easily disturbed and pulled down. (More are shown in Figure S2, Supporting Information.) Another area of failed assembly (blue area) is due to too large width. The dependency map reveals that the bigger the width is, the more difficult assembly forms because of the smaller  $F_c$ . And, a large length is beneficial for assembly (gray area). As shown in Figure 2c–e, straight microchannels with length of 200 μm are built in this way. Owing to the flexibility of laser printing, LC-CFA microchannels with different lengths, widths and heights can be realized conveniently (more information can be found in Figures S3 and S4, Supporting Information).

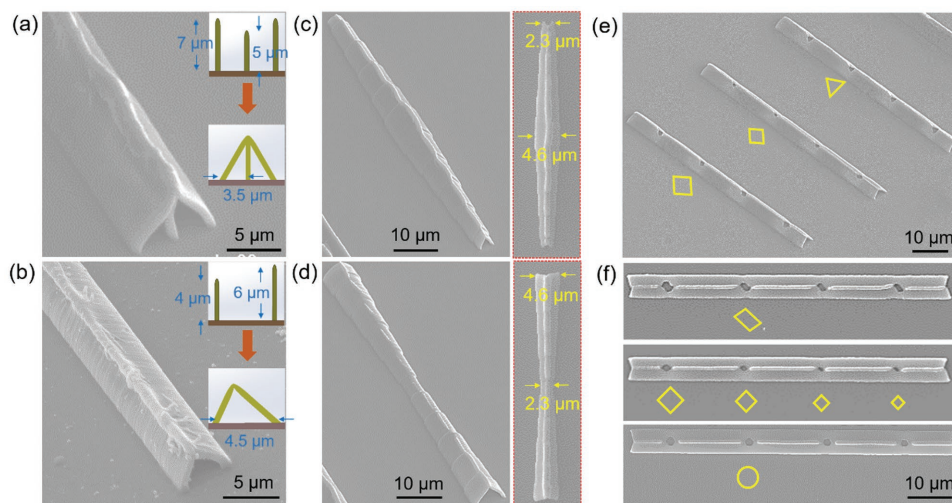
Capillaries pervade human body and transport nutrients as well as metabolites for human physiological activities. Bionic capillaries will enable us to mimic the biochemical reaction on chip and set up tubular microenvironment to culture cells or tissues. However, capillaries are difficult to construct because of their complex patterns, single cell wall and variable sizes. More importantly, there always are a lot of nanoholes or irregular intercellular gaps on the surface of capillaries so as to better exchange nutrients and waste substances with surrounding tissues. Specially, in many cancerous vessels and capillaries surrounded by tumorous or cancerous tissues, there are more and larger holes on the vascular walls than normal vessels. So, microchannel with changeable sizes and designable nanoholes can be used to imitate vessels with thrombus or tumor on chip and may find other special applications in the research of cancerous vessels, cells' behaviors in restricted



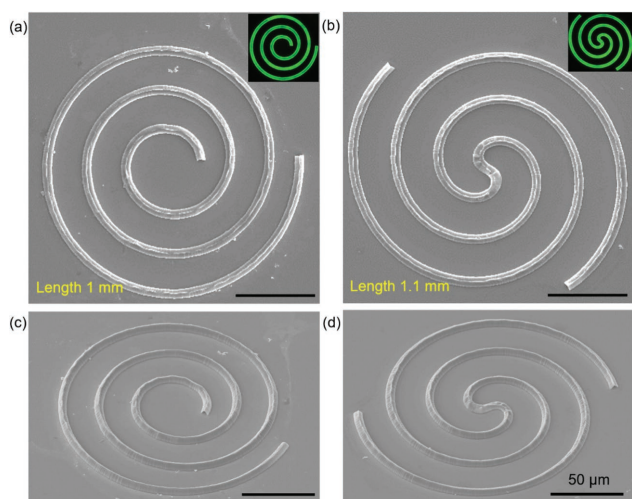
**Figure 2.** Self-assembled microchannels with controllable width, thickness, and length. a) The line chart shows the thickness of the micro wall influenced by laser printing energy and single point exposure time. Inset schematic shows the factors of a microchannel: the length ( $L$ ), height ( $H$ ), thickness ( $t$ ), and width ( $W$ ). b) The dependency map of two microwalls' assembly on ( $L$ ) and ( $W$ ) when  $H$  and  $t$  are fixed (here,  $H \approx 4.5 \mu\text{m}$ ,  $t \approx 700 \text{ nm}$ ). This map was divided into three areas in which the insets are typical images of different experimental results corresponding to the places pointed by arrows. A larger length is conducive to channel's assembly and stability in solutions. The c) optical, d) fluorescence, and e) SEM images of microchannel with  $200 \mu\text{m}$  length. c,d) Scale bars:  $20 \mu\text{m}$ .

micro environment as well as particles or cells filtering. Nevertheless, the fabrication of microchannels with designable holes, long length and thin wall is a technical difficulty for other fabrications. Here, the combination of LC-CFA and laser printing can enable us to overcome these obstacles in the realization of such microchannels. **Figure 3a,b** exhibits the SEM and sketch images of paratactic and tilted microchannels, respectively. As shown in Figure 3a, three walls, among which a shorter one

locates in the middle of two higher walls, collapse together and form two adjacent channels. Moreover, a single channel with varied cross-sections can also be fabricated (Figure 3c,d). First, two walls with changeable height are printed, whose distance are well regulated as shown in insets of Figure 2a. If the heights of the walls match the distance between two walls well, microwalls can assembly into channels with varied widths after developer evaporates. (More details are shown in



**Figure 3.** Microchannels with diverse cross section and designable nanoholes, which is useful in bionic engineering. a,b) Paratactic and tilted microchannel, insets are corresponding schematic diagrams of their cross sections. c, d) Microchannels with changed widths are shown in tilted and top view. e,f) Microchannels with different designable sizes ( $<1$  to  $\approx 3 \mu\text{m}$ ) and patterns (triangle, square, and circle) of nanoholes. The shapes are shown next to the corresponding microchannels with yellow graphics. All tilted angle,  $45^\circ$ . Scale bars: a,b)  $5 \mu\text{m}$ , c–e)  $10 \mu\text{m}$ .



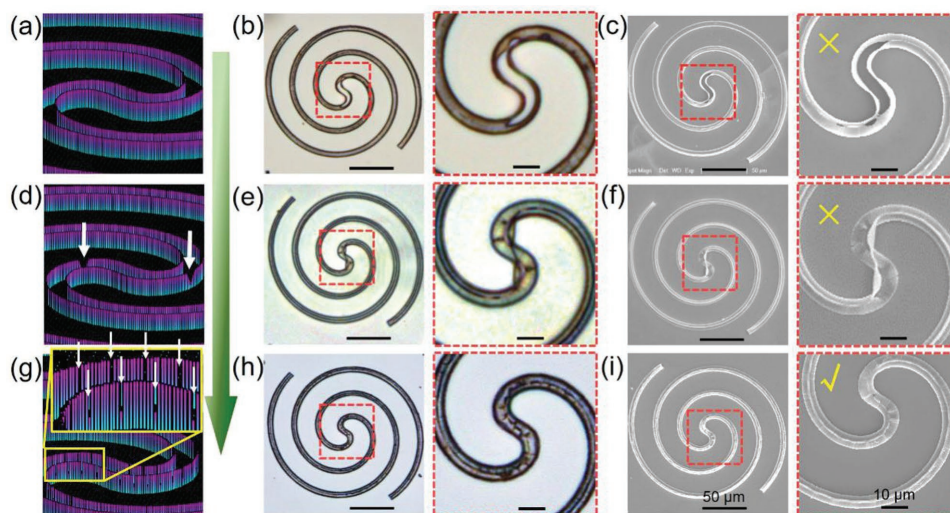
**Figure 4.** Long and complex sealed microchannels fabricated by LC-CFA method without any bonding process. As marked in figures, their lengths are about a,c) 1 mm and b,d) 1.1 mm, respectively. Insets are their corresponding fluorescence images. All scale bars: 50  $\mu\text{m}$ .

Figure S6, Supporting Information.) For example, in Figure 3c the width (4.6  $\mu\text{m}$ ) in the middle of the channel are twice as much as the one (2.3  $\mu\text{m}$ ) in the ends of the channel which is a simulation of capillaries' variable sizes. Figure 3c–f depict the channels decorated with nanoholes whose shapes (triangle, square, and circle), sizes (from  $\approx 0.3$  to  $\approx 3$   $\mu\text{m}$ ) and locations (on the top or in the middle of the wall) can be well designed (more can be seen in Figures S5–S9, Supporting Information). In these varied channels,  $F_c$ ,  $F_s$ , and  $F_v$  change because of changing parameters according to Equations (1)–(3), which proves the flexibility of this fabrication strategy. It is worth noting that though the cross sections of microchannels fabricated here are mainly triangles, which is useful in some

applications, for example, the separation of microparticles,<sup>[18]</sup> our method can also realize curve cross section by controlling the mechanical strength of microwalls in printing.

Another advantage of this strategy based on LC-CFA is that microchannels with almost arbitrary lengths and patterns can be realized. As a proof-of-concept demonstration, two spiral channels whose total lengths are both larger than 1 mm (**Figure 4**) are obtained. Such a long microchannel with small width less than 10  $\mu\text{m}$  and thin walls smaller than 1  $\mu\text{m}$  is hard to be processed by conventional laser direct writing because it is difficult to remove the unpolymerized resin in the enclosed channel during development. So, the combined method based on “line-contact” strategy is crucial for the availability of such microchannel with long length. As shown in Figure 4a,c, the gradual change in curvature radius of microchannel does not affect the channel's closure because of the elasticity of polymeric materials.

In contrast, a sudden change of the curvature radius in the channel center part usually leads to the fabrication failure of the self-assembled channels (**Figure 5**). The sudden change will generate an internal stress, which restricts microchannel's assembly and results in an open part in the center of channels (Figure 5a–c). In order to release the internal stress, a pillar-defect strategy is adopted to realize complex spiral channels as shown in Figure 5. One pillar-defect strategy is that two big gaps ( $\approx 1.5$   $\mu\text{m}$ ) are designed in the channel center where internal stress is relative large (white arrows in Figure 5d), by which the quality of center part of channels can be slightly improved but some defects still exist (Figure 5e,f). The other modified pillar-defect strategy is that several smaller gaps ( $\approx 0.2$   $\mu\text{m}$ ) (white arrows in Figure 5g) are uniformly introduced in the center of microchannel. By this way, self-sealed microchannel is successfully obtained. From Figure 5h,i, we can see that the center part of self-assembled microchannels is smooth and closed tightly.



**Figure 5.** A pillar-defect strategy designing several small gaps to release the internal stress in the center part of self-assembled microchannels. a,d,g) Sketches of microwalls fabricated by laser printing before collapse. a–c) A sudden change of the curvature radius in the channel center part usually leads to the fabrication failure of the self-assembled channels. d–f) Two big gaps ( $\approx 1.5$   $\mu\text{m}$ ) are designed (white arrows in (d)) to release the internal stress by which the quality of center part of channels can be slightly improved but some defects still exist. g–i) Several smaller gaps ( $\approx 0.2$   $\mu\text{m}$ ) (white arrows in (g)) are uniformly introduced in the center of microchannel. By this way, self-sealed microchannel was successfully obtained. Scale bars: 50  $\mu\text{m}$  and 10  $\mu\text{m}$ .

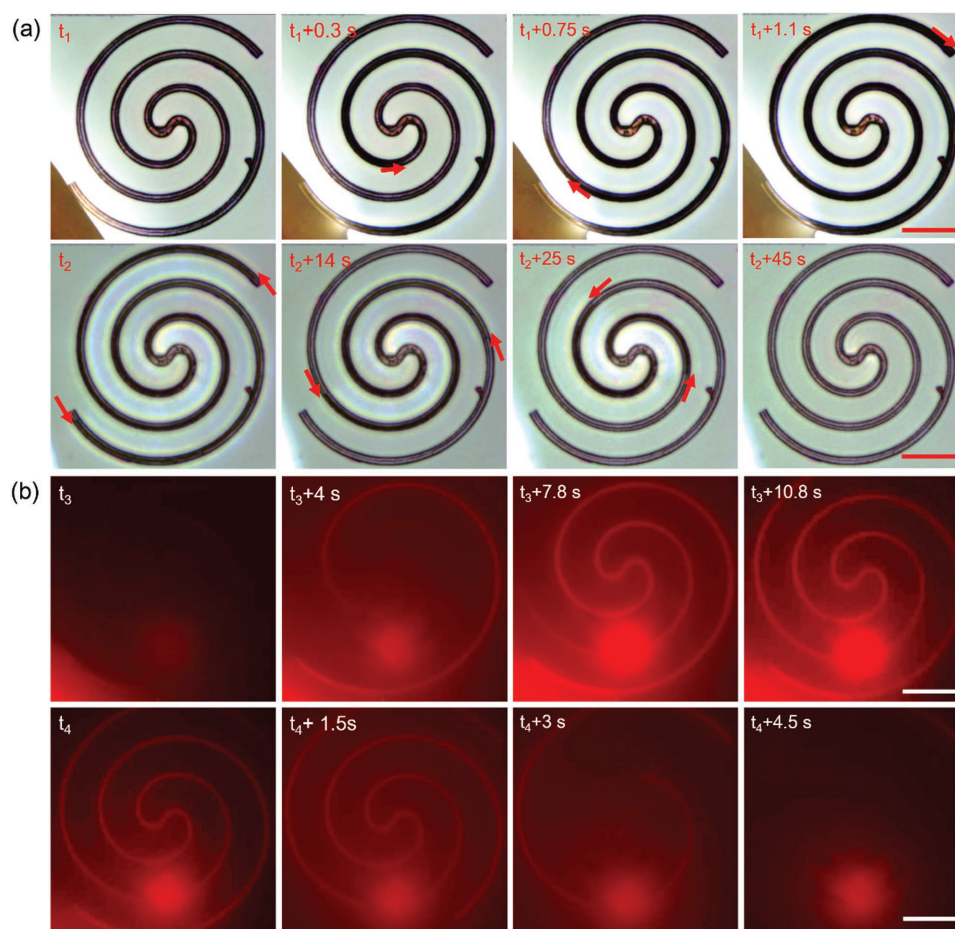


**Figure 6.** The application of self-assembled microchannels as a microfluidic device. a,b) Optical and fluorescence video snapshots. Once the inlet contacts a drop, water will fill the entire microchannel rapidly driven by the capillary force. While removed the drop, the water in channel evaporates slightly slower. The integrity of the waterline proves the good sealing performance of the self-assembled microchannels. Scale bars: 50  $\mu\text{m}$ .

To demonstrate the sealing performance of the LC-CFA channels as a microfluidic device, we conduct experiments on fluid (here, is deionized water) flowing in channels. A droplet is directly dropped closed to the inlet of microchannels on glass slide without any chemical treatment. The contact line of droplet approaches the inlet when drips more water. Water will fill the entire microchannel rapidly (1.1 s) driven by the capillary force as soon as the inlet immersed in the droplet (**Figure 6a**, upper row). Then, the water in microchannel evaporates in 45 s after removing the droplet (more in Video S1, Supporting Information).

In addition, we also dye the water with Rhodamine 6G in order to visualize the channels more distinctly (**Figure 6b**). The flow in the microchannels of water confirms that the LC-CFA channels can be used as a microfluidic device. The ability of microchannel to direct the flow of liquid with capillary force may find applications in microfluidic chemical analyses or biomedical operation free of external pump.

In conclusion, a kind of self-sealed microchannel is realized by the line-contact assembly strategy. The width of microchannels can be reduced to less than 10  $\mu\text{m}$  which means a small volume of lab-chip device and an outstanding advantage for practical applications. Meanwhile, the channels can easily own a length more than 1 mm and a wall

thickness less than 1  $\mu\text{m}$  (similar to human capillaries) which is difficult to be created by other technologies. In particular, nanoholes or microgaps can be fabricated with designable shape, size and location on the channels which is similar to sinusoidal capillaries and cancerous vessels. It should also be mentioned that this method combining fs-laser printing with LC-CFA is extensible which is also suitable for many other materials, e.g., hydrogel, polydimethylsiloxane (PDMS), and even biodegradable materials. We believe that this method will find broad applications in the fields of bionic capillaries or cancerous vessels, tissue engineering, micrototal analysis systems and Lab-on-a-chip systems for biological and chemical analysis researches and so on.

## Experimental Section

**Characterization:** The SEM images were taken by a field emission scanning electron microscope (Sirion 200, FEI). Before imaging, the samples were sputtered with a thin layer ( $\approx 10$  nm) of gold. The fluorescent images of the structures were taken by an inverted microscope with fluorescence (DMI 3000B, Leica), where an excitation filter of 450–490 nm was used.

*Microfluidic Experiment:* The two videos of the microchannels were recorded by the Leica microscope (DMI 3000B, Leica) in bright-field mode and fluorescence-field mode, respectively. The environment condition was kept  $23 \pm 1$  °C in  $45\% \pm 5\%$  relative humidity. The concentration of Rhodamine 6G aqueous solution used here was about  $0.5 \mu\text{g mL}^{-1}$ .

## Supporting Information

Supporting Information is available from the Wiley Online Library or from the author.

## Acknowledgements

This work was supported by the National Science Foundation of China (Nos. 51275502, 61475149, 61675190, and 51405464), the Anhui Provincial Natural Science Foundation (No. 1408085ME104), the Fundamental Research Funds for the Central Universities (WK2480000002 and WK6030000004), and the Chinese Thousand Young Talents Program.

## Conflict of Interest

The authors declare no conflict of interest.

- [1] S. H. Au, B. D. Storey, J. C. Moore, Q. Tang, Y. L. Chen, S. Javaid, A. F. Sarioglu, R. Sullivan, M. W. Madden, R. O'Keefe, D. A. Haber, S. Maheswaran, D. M. Langenau, S. L. Stott, M. Toner, *Proc. Natl. Acad. Sci. USA* **2016**, *113*, 4947.
- [2] K. S. Toohey, N. R. Sottos, J. A. Lewis, J. S. Moore, S. R. White, *Nat. Mater.* **2007**, *6*, 581.
- [3] a) G. Huang, Y. Mei, D. J. Thurmer, E. Coric, O. G. Schmidt, *Lab Chip* **2009**, *9*, 263; b) C. Norotte, F. S. Marga, L. E. Niklason, G. Forgacs, *Biomaterials* **2009**, *30*, 5910; c) K. Sarveswaran, V. Kurz, Z. Dong, T. Tanaka, S. Penny, G. Timp, *Sci. Rep.* **2016**, *6*, 21885.
- [4] a) D. J. Thurmer, C. Deneke, Y. F. Mei, O. G. Schmidt, *Appl. Phys. Lett.* **2006**, *89*, 223507; b) B. Xu, W. Q. Du, J. W. Li, Y. L. Hu, L. Yang, C. C. Zhang, G. Q. Li, Z. X. Lao, J. C. Ni, J. R. Chu, *Sci. Rep.* **2016**, *6*, 19989; c) X. Hou, *Design, Fabrication, Properties and Applications of Smart and Advanced Materials*, CRC Press, Boca Raton, FL **2016**; d) D. Wu, J. Xu, L. G. Niu, S. Z. Wu, K. Midorikawa, K. Sugioka, *Light: Sci. Appl.* **2015**, *4*, e228; e) X. Hou, Y. H. Hu, A. Grinthal, M. Khan, J. Aizenberg, *Nature* **2015**, *519*, 70; f) X. Hou, *Adv. Mater.* **2016**, *28*, 7049.
- [5] Y. L. Zhang, Q. D. Chen, H. Xia, H. B. Sun, *Nano Today* **2010**, *5*, 435.
- [6] Y. F. Mei, A. A. Solovev, S. I. Sanchez, O. G. Schmidt, *Chem. Soc. Rev.* **2011**, *40*, 2109.
- [7] a) E. J. Smith, S. Schulze, S. Kiravittaya, Y. F. Mei, S. Sanchez, O. G. Schmidt, *Nano Lett.* **2010**, *11*, 4037; b) S. Sánchez, *Lab Chip* **2015**, *15*, 610; c) D. Wu, L. G. Niu, S. Z. Wu, J. Xu, K. Midorikawa, K. Sugioka, *Lab Chip* **2015**, *15*, 1515.
- [8] D. P. Parekh, C. Ladd, L. Panich, K. Moussa, M. D. Dickey, *Lab Chip* **2016**, *16*, 1812.
- [9] a) K. M. Stroka, H. Jiang, S. H. Chen, Z. Tong, D. Wirtz, S. X. Sun, K. Konstantopoulos, *Cell* **2014**, *157*, 611; b) W. Xi, C. K. Schmidt, S. Sanchez, D. H. Gracias, R. E. Carazo-Salas, S. P. Jackson, O. G. Schmidt, *Nano Lett.* **2014**, *14*, 4197.
- [10] Y. Huang, P. Froeter, O. V. Cangelaris, W. Huang, E. W. Dent, M. U. Gillette, J. C. Williams, X. L. Li, *Acs Nano* **2014**, *8*, 11108.
- [11] a) B. B. Xu, Y. L. Zhang, H. Xia, W. F. Dong, H. Ding, H. B. Sun, *Lab Chip* **2013**, *13*, 1677; b) D. Wu, S. Z. Wu, J. Xu, L. G. Niu, K. Midorikawa, K. Sugioka, *Laser Photonics Rev.* **2014**, *8*, 458.
- [12] a) S. Lee, G. S. Jeong, J. Kim, J. Yoon, S. Han, J. Y. Kang, S. Chung, S. H. Lee, *Microsyst. Technol.* **2012**, *19*, 1025; b) X. H. Tan, T. L. Shi, Y. Gao, W. J. Sheng, B. Sun, G. L. Liao, *J. Micromech. Microeng.* **2014**, *24*, 055006; c) S. Tian, X. Xia, W. Sun, W. Li, J. Li, C. Gu, *Nanotechnology* **2011**, *22*, 395301.
- [13] a) E. Stankevicius, T. Gertus, M. Rutkauskas, M. Gedvilas, G. Raciukaitis, R. Gadonas, V. Smilgevicius, M. Malinauskas, *J. Micromech. Microeng.* **2012**, *22*, 065022; b) L. Yang, A. El-Tamer, U. Hinze, J. W. Li, Y. L. Hu, W. H. Huang, J. R. Chu, B. N. Chichkov, *Appl. Phys. Lett.* **2014**, *105*, 041110; c) C. C. Zhang, Y. L. Hu, J. W. Li, G. Q. Li, J. Chu, W. Huang, *Opt. Express* **2014**, *22*, 3983.
- [14] a) B. Pokroy, S. H. Kang, L. Mahadevan, J. Aizenberg, *Science* **2009**, *323*, 237; b) D. Chandra, S. Yang, *Acc. Chem. Res.* **2010**, *43*, 1080.
- [15] H. Duan, J. K. Yang, K. K. Berggren, *Small* **2011**, *7*, 2661.
- [16] D. Wu, S. Z. Wu, S. Zhao, J. Yao, J. N. Wang, Q. D. Chen, H. B. Sun, *Small* **2013**, *9*, 760.
- [17] Sidorenko, T. Krupenkin, A. Taylor, P. Fratzl, J. Aizenberg, *Science* **2007**, *315*, 487.
- [18] Y. L. Hu, Z. X. Lao, Benjamin P. Cumming, D. Wu, J. W. Li, H. Y. Liang, J. R. Chu, W. H. Huang, M. Gu, *Proc. Natl. Acad. Sci. USA* **2015**, *112*, 6876.
- [19] Z. X. Lao, Y. L. Hu, C. C. Zhang, L. Yang, J. W. Li, J. R. Chu, D. Wu, *ACS Nano* **2015**, *9*, 12060.

Received: November 25, 2016  
Revised: March 13, 2017  
Published online: April 25, 2017